Construction and Building Materials

Manufacture of rich-sulfoaluminate belite cement at low temperature from waste mixture by dry and hydrothermal processes

--Manuscript Draft--

Manuscript Number:	CONBUILDMAT-D-21-07561R3
Article Type:	Research Paper
Keywords:	Eco-cement, Sulfoaluminate cement, Hydrothermal treatment, Clinkering process, Mineral wastes, Hydraulic properties
Corresponding Author:	Larbi KACIMI, Professor Université des Sciences et de la Technologie d'Oran Mohamed Boudiaf: Universite des Sciences et de la Technologie d'Oran Mohamed Boudiaf Oran, ALGERIA
First Author:	Faiza Nabila Bouha, Doctor
Order of Authors:	Faiza Nabila Bouha, Doctor
	Larbi KACIMI, Professor
	Angeles G De la Torre, Professor
Abstract:	This study, within the framework of eco-cement development, aims to manufacture reactive belite-sulfoaluminate cement (BYF) as alternative to Portland cement (PC). This ecological cement is obtained at low temperature from a mixture of industrial wastes using two synthetic methods, dry and hydrothermal treatment. The main minerals of this cement are β-C2S and calcium sulfoaluminate (C4A3Š), the latter being very reactive, which provide high performances cementitious materials. The hydrothermal treatment of raw mixture led to reduce the burning temperature of clinker up to 1200°C. The mineral phases of the produced cements and theirs pastes were identified and quantified by XRPD coupled with Rietveld method. The hydraulic reactivity of cement was studied using XRPD and thermal analyses. The resulting mortars are very reactive and develop more than 42 MPa of compressive strengths after 28 days.
Suggested Reviewers:	Abdelhak KACI, Professor Professor, Cergy-Pontoise University: CY Cergy Paris Universite abdelhak.kaci@cyu.fr Professor Researcher very competent in the fields of cements and concretes
	Ana Guerrero, Professor Professor, ICMM-CSIC: Instituto de Ciencia de Materiales de Madrid ana.guerrero@csic.es Professor Researcher very competent in the fields of cement and geopolymer
	Aurora López-Delgado, Professor Professor, National Council for Research: National Centre for Research alopezdelgado@cenim.csic.es Professor Researcher very competent in the fields of cement, zeolithe and geopolymer
	Patrick Rousseaux, Professor Professor, Poitiers University: Universite de Poitiers patrick.rousseaux@univ-poitiers.fr Professor Researcher very competent in the field of reaction process in mineral compounds
	Pierre Clastres, Professor Professor, Institut National des Sciences Appliquees de Toulouse: INSA Toulouse clastres@insa-toulouse.fr Professor Researcher very competent in the fields of cements, concretes, binders and geopolymers

Manufacture of rich-sulfoaluminate belite cement at low temperature from waste mixture by dry and hydrothermal processes

Faiza Nabila Bouha [1], Larbi Kacimi [1*], Angeles G. De la Torre [2]

[1] Laboratoire des Eco-Matériaux Fonctionnels et Nanostructurés (LEMFN), Faculté de Chimie, Université des Sciences et de la Technologie d'Oran- Mohamed Boudiaf, Algeria.
* E.Mail : kacimi20002000@yahoo.fr Tel. +213 560539975 Fax. +213 41627172
[2] Dpt. Química Inorgánica, Cristalografía y Mineralogía, Facultad de Ciencias, Universidad de Málaga
E.Mail: mgd@uma.es Tel. +34 952131877

Abstract

This study, within the framework of eco-cement development, aims to manufacture reactive belite-sulfoaluminate cement (BYF) as alternative to Portland cement (PC). This ecological cement is obtained at low temperature from a mixture of industrial wastes using two synthetic methods, dry and hydrothermal treatment. The main minerals of this cement are β-C_2S and calcium sulfoaluminate ($C_4A_3\check{S}$), the latter being very reactive, which provide high performances cementitious materials. The hydrothermal treatment of raw mixture led to reduce the burning temperature of clinker up to 1200°C.

The mineral phases of the produced cements and theirs pastes were identified and quantified by XRPD coupled with Rietveld method. The hydraulic reactivity of cement was studied using XRPD and thermal analyses. The resulting mortars are very reactive and develop more than 42 MPa of compressive strengths after 28 days.

Keywords: Eco-cement, Sulfoaluminate cement, Hydrothermal treatment, Clinkering process, Mineral wastes, Hydraulic properties.

1. Introduction

The adverse environmental aspect of the cement manufacturing, related to the strong CO_2 emission [1], is a major concern of researchers and the international community, although the high demand of this conventional material. One alternative is to replace globally the Portland cement (PC) by low-carbon binders that are not based on Portland clinker and so, require less manufacturing temperature [2–7]. The promoter green cement is the Calcium Sulfo-Aluminate Cement (CSA) which contains the calcium sulfoaluminate phase ($C_4A_3\check{S}$) known by its high hydraulic reactivity. Due to its environmental benefits, this type of ecological cement has recently emerged to replace the conventional cement. For its production, this cement requires a low limestone and high alumina raw materials and low burning temperature (~1250°C), about 200°C lower than PC, which minimizes the CO_2 emissions.

The calcium sulfoaluminate cements (CSA) are numerous and differ according to their main crystalline phases [8–10]. Recently, Belite-rich-Sulfo-Aluminate Cements, also known as Belite-Ye'elimite-Ferrite (BYF) cements, have been identified in recent studies as a potential substitute for PC on a large production scale [11–13]. BYF cements are based on belite (C_2S), calcium sulphoaluminate ($C_4A_3\check{S}$), also called "ye'elimite" or "Klein's" salt [14,15], ferrite (C_4AF) and calcium sulfate ($C\check{S}$) [16–20]. In the manufacturing of BYF, the used raw materials must contain a significant amount of sulfate and alumina, usually derived from gypsum and bauxite, in addition to limestone, clay and iron ore. However, the industrial by-products and wastes are emerging as alternative raw materials for the BYF manufacture, such as fly ash, steel slag, flue gas desulfurization sludge (FGDS) and phosphogypsum.

Several studies have focused on the use of various inorganic industrial wastes to produce BYF cements. Chen et al. [21] prepared BYF clinker from industrial wastes such as fly ash, flue gas desulfurization sludge and fluidized bed ash, by clinkering at 1250°C to obtain $C_4A_3\check{S}$, C_2S, C_4AF and $C\check{S}$ minerals. Arjunan et al. [20] reported that BYF clinker could be synthesized from fly ash, bag house dust and scrubber sludge at around 1250°C if the raw mixture is used as nodules and at 1175°C as powder. El-Alfi and Gado [13] used the marble sludge waste, kaolin and hemihydrates to prepare BYF cement at 1200°C. Its mineral composition calculated using the modified Bogue equations is: 22.3 wt% of $C_4A_3\check{S}$, 43.6 wt% of C_2S, 1.6 wt% of C_4AF, 18.6 wt% of $C\check{S}$ and 3.8 wt% of free lime. The compressive strength of this cement was about 36 MPa after 28 days. Isteri et al. [22] prepared a BYF type cement composed from ye'elimite, belite and ferrite, by burning at 1300°C a mixture of steel industry residues: argon oxygen decarburization slag resulting from the steel refining process, fayalitic slag from the nickel flash furnace process, and iron slag from the pyrometallurgically

treated jarosite. Da Costa et al. [23] used aluminum anodizing sludge as Al_2O_3 source, calcium sulfate and limestone to produce BYF cement at 1250°C. The compressive strength of the cement mortar was 41.7 MPa after 28 days of hydration.

BYF clinkers are usually manufactured in rotary kilns at burning temperatures ranging from 1300 and 1350°C. In this work, a considerable interest is devoted to the synthesis of BYF clinker using the hydrothermal process to reduce the burning temperature. Hydrothermal synthesis method is a chemical reaction process in heterogeneous solution with aqueous or non-aqueous solvent, autoclaved under heating and pressure [24]. This method was used for the first time to synthesize a high reactive belite phase (α'_L-C_2S) [25–28]. However, there is less research on the hydrothermal synthesis of BYF clinker. Rungchet et al. [29] used the hydrothermal-calcination method to produce a calcium sulfoaluminate belite cement at 1050°C. The obtained cement was manufactured from mixture of industrial wastes (fly ash, Al-rich sludge and flue gas desulfurization gypsum) and was composed from belite, ye'elimite, mayenite and ferrite. The hydrothermal treatment was performed using autoclave at 130°C. Various factors, namely the time of hydrothermal treatment, the solvent nature (NaOH and H_2O) and the calcination temperature were investigated.

The hydration of BYF cement is related to the mineralogical composition of the binder, the amount and type of the added calcium sulphate (anhydrite, hemihydrate or gypsum) and the water to cement ratio, w/c [30]. Ye'elimite ($C_4A_3\check{S}$) reacts immediately when water is added in presence of calcium sulfate leading to the formation of ettringite (AFt) according to equation (1). Without calcium sulfate, $C_4A_3\check{S}$ reacts to form AFm phase ($C_4A\check{S}H_{12}$) according to equation (2). The ratio between ettringite and monosulfate in the BYF paste is related to the ratio between ye'elimite and calcium sulfate in cement [31,32]. The formation of ettringite promotes the high early strength and the rapid setting of BYF cement.

$$C_4A_3\check{S} + 2\ C\check{S}H_n + (38\text{-}2n)\ H \longrightarrow C_6A\check{S}_3H_{32} + 2\ AH_3 \quad \text{..... (1)}$$

$$C_4A_3\check{S} + 18\ H \longrightarrow C_4A\check{S}H_{12} + 2\ AH_3 \quad \text{..... (2)}$$

The main objective of the present work is to produce very reactive sulfoaluminate belitecement (BYF) of high mechanical performances, at low temperature, using the hydrothermal-calcination method and valorizing industrial wastes (hydraulic dam sludge, slaked lime dust and iron ore).

2. Materials and methods

2.1. Raw materials

The raw mixture used to synthesize BYF cement was composed from industrial wastes and natural materials. The used wastes were hydraulic dam sludge (SLD), collected from Brizina dam in Algeria, slaked lime dust (LD) recovered from lime bagging workshops of Saida lime plant in Algeria and iron compound (IO) which is a by-product of sulfuric acid industry in Spain. The gypsum ore (GS) was collected from natural deposit of Chlef in Algeria. The alumina deficiency was compensated by adding a pure aluminum oxide (PA) (purity > 99%), from Honeywell-Fluka. The raw materials were dried in a stove at 105°C and then crushed to 80 µm. The chemical composition carried out by X-ray fluorescence (XRF), and the mineralogical composition, determined by X-ray diffraction (XRPD), of the raw materials are given in Table 1 and Figure 1, respectively. Table 2 gives the crystal structures used as references to perform Rietveld refinement. It gives nomenclatures, designations, chemical formulas and ICSD card numbers of the mineral phases contained in the raw materials and synthesized cements.

2.2. Synthesis procedure

To synthesize BYF clinkers, two processes steps were followed: the activation of the raw mixture by hydrothermal method and the clinkering by heating process. After the calculation of the raw material dosification (Table 3) was homogenized in a micro-Deval machine for 30 min with a rate of 100 rpm and then activated using the hydrothermal method in deionized water with a liquid to solid ratio of 5. This hydrothermal precursor (hereafter HT-BYF), stirred for 4 hours at 100°C under atmospheric pressure in a closed container, was filtered and dried in oven at 60°C for 24 h. The dry method was also employed to prepare another cement (hereafter DM-BYF), which consist on mixing and homogenizing the raw materials after crushing separately to 80 µm and calculation. DM-BYF was prepared without hydrothermal treatment and used as control sample. The second stage of the synthesis process was the burning of the dried precursor to 900°C, with a heating rate of 10°C/min, and then to the final temperature (1100-1300°C) with 5 °C/min during 30 minutes, followed by rapid air-cooling. The obtained clinkers were named “DM-BYF-1300”, for the control sample burned at 1300°C prepared by dry method, and “HT-BYF 1100”, “HT-BYF-1200”, “HT-BYF-1250” and “HT-BYF-1300” for the products burned at 1100, 1200, 1250 and 1300°C, respectively, prepared by hydrothermal method.

Cement samples of DM-BYF and HT-BYF were prepared by mixing the obtained clinker and anhydrite ($CaSO_4$) with stoichiometric proportions in micro-Deval machine of 100 rpm for 30 minutes. The anhydrite was prepared by heating, at 700°C for 60 min, commercial basanite from BELITH S.P.R.L. (Belgium).

Cement paste samples were prepared with deionized water using water to cement mass ratio (w/c) of 0.5, according to EN 193-1 standard. The pastes were poured into hermetically sealed cylindrical molds and then stored at room temperature (20±1°C) for 24 hours [33]. Afterwards, the samples were demolded and stored in deionized water at room temperature for testing after 1, 3, 7, 14 and 28 days of hardening. To stop the hydration process until the characterization time, the paste samples were manually ground and washed twice with isopropanol, once with diethyl ether and finally the powders were dried at 40ºC for 24 hours in a stove.

2.3. Sample testing

The chemical compositions of raw materials and synthesized clinkers, crushed to 80 μm, were determined by X-ray fluorescence (XRF) using an AL ADVANT'XP Thermo Fisher equipment. The mineralogical compositions of raw materials, clinkers and cement pastes were performed by X Ray Powder Diffraction (XRPD) in a X'Pert MPD PRO diffractometer (PANalytical) using monochromatic CuKα_1 radiation (λ= 54059Å, Ge (111) primary monochromator) and X'Celerator detector. Data and powder patterns were recorded in Bragg-Brentano reflection configuration by using PIXcel 3D detector from 5 to 70°/2θ, with step scan of 0.017°. Quartz (SiO_2, 99.5% Alfa Aesar) was used as internal standard and ~20 wt% was mixed with samples to determine the amorphous and non-quantified crystalline phases (ACn) contents [34,35]. The crystalline phase amounts were determined by Rietveld method using HighScore Plus software (v 3.5) from PANAlytical. Thermo-gravimetric analysis and differential scanning calorimetry (TGA/DSC) were carried out in a SDT-Q600 analyzer from TA instruments with heating rate of 10 °C/min up to 1000°C under air flow. Isothermal calorimetric analysis was performed in an eight channel TAM Air Isothermal conduction calorimetry of TA Instruments, to study the cement paste hydration at early age. The mineral phase morphology of clinkers and cement pastes was examined by a JEOL JSM-6490LV scanning electron microscope on a grain (≈ 5 mm of size) vacuum metalized with graphite. The specific surface area of the anhydrous cements was calculated from the sorption isotherm data using BET (Brunauer-Emmett-Teller) method on an automatic MICROMERITICS ASAP 2020 at low partial pressures of the inert gas (N_2, 77 K). The surface specific area was also calculated

using Blaine method. To determine the compressive strength of the synthesized cements at various hardening ages, mechanical tests were carried out on standardized mortar specimens (4x4x16 cm^3) prepared at room temperature with water to cement ratio (w/c) of 0.5 and sand to cement ratio of 3:1, according to EN 196-1 standard.

3. Results and discussion

3.1. Preparation of the raw mixture and hydrothermal precursor of BYF cement

The hydrothermal precursor of BYF cement (HT) was obtained by hydrothermal treatment of raw material mixture according to the proportions indicated in Table 3. Another mixture of similar composition but prepared by dry process (DM) was studied as control sample to be compared with the HT clinker. After crushing to 80 microns the DM and HT raw mixtures were analyzed by XRPD to determine their mineralogical compositions. The quantitative composition of crystalline mineral phases in both mixtures was determined by Rietveld method. TGA analysis was also used to show the formation of some hydrates in the precursor obtained by hydrothermal treatment. The results are shown in Figures 2, 3 and Table 4. The mixtures were composed mainly of the starting minerals, quartz, calcite, muscovite, dolomite, gypsum, portlandite, corundum and hematite (Figure 2). However, a difference in the main peak intensities of gypsum and corundum between both mixtures was observed (Figure 2). This difference is shown by the decrease in gypsum, portlandite and corundum amounts, determined by Rietveld method (Table 4), and the formation of kuzelite ($C_4AŠH_{12}$). The amount of muscovite decreases after hydrothermal treatment, which was due to the amorphization of part of this mineral to form C-S-H gel. The formation of kuzelite and C-S-H gel by the hydrothermal treatment were confirmed by TGA analysis (Figure 3). The decrease in the peak intensities of portlandite and quartz in the hydrothermal mixture pattern (Figure 4) is mainly due to the pozzolanic reaction producing C-S-H mineral [27,28]. The formation of C-S-H amorphous mineral leads to the improvement of the clinkering process of hydrothermal mixture [27,28]. An increase in the calculated percentages of quartz and calcite for HT mixture was observed (Table 4), which could be explained by a decrease in the crystalline mass of the analyzed sample because Rietveld method calculation takes into account only the crystalline phases that detected by XRPD. This testifies that the amorphous phase amounts of C-S-H, C-A-S-H and/or C-A-Š-H gels increase, due to the hydrothermal treatment, enhancing the formation of BYF clinker phases at low temperature during the burning process [25–28], see next section.

3.2. Synthesis of BYF clinker from hydrothermal and dry mixtures

Both mixtures (DM and HT) were clinkered at various temperatures, 1100, 1200, 1250 and 1300°C, with a heating rate of 10 °C/min up to 900°C for 30 minutes and 5 °C/min thereafter, following by rapid air-cooling. The obtained clinkers at different burning temperatures were analyzed by XRPD after crushing to 40 μm. Figure 4 shows the patterns of the obtained clinkers. Table 5 reports their mineralogical compositions determined by Rietveld method.

These results (Figure 4, Table 5) showed that all clinkers were composed of belite (β-C_2S), ye'elimite ($C_4A_3\check{S}$), with cubic and orthorhombic polymorphs, and ferrite (C_4AF). In addition to these main BYF clinker phases, mayenite ($C_{12}A_7$), which was not present in DM-BYF-1300 clinker, was also found beside an insignificant amount of MgO in HT-BYF-1200 clinker. No-presence of anhydrite ($CaSO_4$) or free lime (CaO) was observed in any of the clinkers (Figure 4 and Table 5) which testifies that the clinkering procedure was finished. The mineralogical compositions of the obtained products reveal that the burning and cooling processes of clinkers were successfully performed. It should be noted that the clinker obtained at temperature lower than 1300°C without hydrothermal treatment of raw mixture (DM) had contained an important amounts of no-combined lime and quartz, which testifies the incomplete clinkering of the product. Consequently, 1300ºC was considered the minimum temperature to obtain BYF clinker with the dry methodology, where quartz remains in a very small amount (Figure 4, Table 5). However, the disappearance of quartz and free lime from the burned HT mixture, even at low temperature (1100°C), shows that the hydrothermal treatment allows a complete and rapid combination between oxides, having acquired a chemical activity, to form BYF clinker at low temperature.

Table 5 gives information about the influence of temperature on phase assemblage. Belite (β-C_2S) amount decreases and the amounts of calcium sulfoaluminate phases (c-$C_4A_3\check{S}$, o-$C_4A_3\check{S}$) and C_4AF increase when the burning temperature increases from 1100 to 1300°C. The hydrothermal treatment allows the formation of high amount of belite at low temperature (1100°C) which is due the activation of the grain surface of quartz and calcium compounds yielding to a rapid formation of C-S-H (Figure 3) that quickly decomposed into β-C_2S belite phase at low temperatures [25–28]. The hydrothermal activation of mixture allowed also the formation of an amorphous and highly reactive phase rich in alumina, sulphate, hematite and calcium which crystallizes into $C_4A_3\check{S}$ phases and C_4AF at low burning temperature (1100°C) to increase rapidly by forming high amounts at 1200°C [29]. The increase of these mineral phase amounts with the burning temperature is due to their crystallisation from the gel during the heating process. The higher amounts of reactive phases [28,29,36], i.e. o-$C_4A_3\check{S}$, c-$C_4A_3\check{S}$,

$C_{12}A_7$ and C_4AF, in HT-BYF-1200 clinker compared to DM-BYF-1300 is related to the formation of amorphous material during the hydrothermal treatment of raw mixture. The mineralogical composition of HT-BYF-1200 is close to the targeted one, consequently, it will be used to prepare BYF cement and to continue with the hydration study.

3.3. Chemical and physical properties of the synthesized BYF clinkers

HT-BYF-1200 and DM-BYF-1300 clinkers were further characterized. The results of the chemical compositions, carried out by XRF analysis, the density and the specific surface area (SSA), determined by Blaine and BET methods, of these clinkers are given in Tables 6 and 7.

The chemical composition of the clinker HT-BYF-1200 was similar to that of BYF clinker obtained at 1300°C by dry method (DM-BYF-1300), as expected since the raw materials dosification is the same. Although their similar densities, their surface specific area was different, in spite of having being milled them in the same way, i.e. in a ball mill during 20 minutes. It was observed that the surface specific area (SSA), determined by Blaine or BET method was higher in the case of HT-BYF-1200 clinker. It should be noted that Blaine method is a macroscopic technique which gives SSA related to the particle size of material, while BET is a microscopic method providing information about the material porosity. Thereby, the SAA-BET low value of DM-BYF-1300 shows that this clinker was more compact than HT-BYF-1200 and also that the particle sizes are bigger. In the clinkering process of DM-BYF-1300, a larger fraction of melted phases should have appeared since the amorphous fraction of this clinker is higher than that of HT-BYF-1200, Tables 8, 9. The higher amorphous fraction, coming from a melted material at high temperature, makes this clinker harder to be milled and it is responsible of the lower value of SSA-Blaine, which is traduced by higher particle size of DM-BYF-1300 than HT-BYF-1200 after their crushing in a ball mill for the same time (20 minutes) [37,38].

3.4. Hydration study of cement pastes of the synthesized clinkers

HT-BYF-1200 and DM-BYF-1300 clinkers were mixed with 13 wt% and 10 wt% of anhydrite, respectively. The added anhydrite percentages were calculated according to ye'elimite and mayenite content in each clinker, taking into account the formation of ettringite reactions. From these cements, pastes were prepared with w/c of 0.5.

3.4.1. XRPD characterization of HT-BYF-1200 and DM-BYF-1300 cement pastes

The phase evolution of HT-BYF-1200 and DM-BYF-1300 cement pastes with hydration time was followed by XRPD and the Rietveld method at 1, 3, 7, 14 and 28 days of hydration. The hydration process was stopped as mentioned in the experimental section. The results are shown in Figures 5 and 6 and Tables 8 and 9. It should be noted that the amorphous phase (ACn) and free water (FW) amounts in cement pastes were calculated using the internal standard method (Q in Figure 5 and 6, stands for quartz added as internal standard) and TGA analysis, respectively. Figures S1 and S2, deposited as supplementary information, give the Rietveld plots of HT-BYF-1200 and DM-BYF-1300 after 28 days of hydration.

It was observed that the nature of hydration products was the same for both cement pastes, and the main hydrated mineral was ettringite (AFt) (Figures 5, 6). The amorphous phase amount before starting hydration is higher in DM-BYF-1300 cement (Tables 8, 9), which confirms that its clinker contains more vitreous phase than HT-BYF-1200. The hydration process is more rapid for the HT-BYF-1200 than DM-BYF-1300 cement. In HT-BYF-1200 cement paste, the amounts of anhydrous minerals (β-C_2S, $C_4A_3\check{S}$, C_4AF, $C_{12}A_7$, $C\check{S}$, MgO) decrease rapidly with hardening age to form high amounts of hydration products (AFt and ACn). The disappearance of ye'elimite phases (c-$C_4A_3\check{S}$ and o-$C_4A_3\check{S}$) from the cement paste after one day only of hardening and anhydrite ($C\check{S}$) after 3 days is due to their very rapid and complete transformation to form high amounts of ettringite (AFt) (Table 8) and amorphous gibbsite (AH_3) according to the chemical reaction (1). AH_3 used to present nanoparticles [39] and consequently is not observed in XRPD (Figure 5). This lead to increase the amorphous hydrate phase (ACn) also containing other amorphous products like calcium silicate hydrate (C-S-H), calcium aluminosilicate hydrate (C-S-A-H) or hydrogarnet phases resulting from the hydration of belite (β-C_2S) and C_4AF minerals, respectively. This was confirmed by the high decrease of free water (FW) after its chemical reactions with anhydrous minerals (Table 8). The presence of free water (10 wt%) even at 28 days of hardening shows that the hydration process was not yet finished, especially for β-C_2S, and so the production of more hydrated products will be continue after this age. These mineral characteristics of cement pastes conduce to the improvement of their mechanical performances.

Mayenite ($C_{12}A_7$), known by its high chemical reactivity, reacts quickly with water at early age of which its amount deceases to very low value after 1 day of hardening (Table 8), after its transformation into ettringite (AFt) and nanocrystalline gibbsite (AH_3), according to chemical equation (3). The rapid formation of this ettringite (equation 3), in addition to that resulting from ye'elimite transformation (equation 1), which deposits and crystallizes on the

grain surface of mayenite, leads to decrease its hydration beyond 1 day of hardening. This may be the reason of the slowness in the belite hydration after coverage of its grain surface by rapid ettringite formation [40,41].

$C_{12}A_7 + 12\ C\check{S} + 137\ H \longrightarrow 4\ C_6A\check{S}_3H_{32} + 3\ AH_3$ ……..(3)

The hydration process of DM-BYF-1300 cement was slower than HT-BYF-1200 cement, although the nature of hydrated products was similar (Figures 5 and 6). The mineral transformation during paste hardening of HT-BYF-1200 proceeded with faster kinetics than DM-BYF-1300, producing more amounts of hydrates like ettringite (AFt) and gel (ACn) (Tables 8, 9). Considering water as a reactant, the degree of reaction of free water can be calculated with equation (4),

$DoR_{phase}(\%) = (wt\%_{t0}-wt\%_{tx})x100 / wt\%_{t0}$……..(4)

where $wt\%_{t0}$ the starting weight percentage of an individual phase, in this case free water and $wt\%_{tx}$ is the amount of that phase at a given hydration time tx, from Tables 8 and 9. Table S1 and S2 (in supplementary materials) give the reaction degree (DoR) of belite and mixing water of HT-BYF-1200 and DM-BYF-1300. After 1 day of hydration, the DoR of mixing water was 55 and 39% for HT-BYF-1200 and DM-BYF-1300 respectively (Table S1 and S2), showing the faster reaction of the former. Mayenite ($C_{12}A_7$), which was not present in DM-BYF-1300, contributed to the formation of more gel (ACn) in HT-BYF-1200 cement paste (Tables 8 and 9). The high presence of amorphous phase (ACn at 0 day) in DM-BYF-1300 (Table 9) compared to HT-BYF-1200 (Table 8), may have inhibited the hydration process and consequently prevented the proper hardening development of cement paste. The DoR of β-C_2S have been also calculated (Table S1 and S2), being 63 and 34% for HT-BYF-1200 and DM-BYF-1300 pastes respectively after 28 days of hydration, showing that this phase has reacted at a higher pace in the former.

The higher hydration degree of HT-BYF-1200 cement compared to DM-BYF-1300 was due to the hydrothermal treatment of raw mixture conducing to the formation of highly reactive minerals at low burning temperatures (1200°C). The increase of this temperature to 1300°C for the case of DM-BYF-1300 clinker conduced to a decrease in mineral reactivity and produced high amount of vitreous phases, which are unfavorable for hydration and hardening process of cement paste.

3.4.2. Thermal analysis of HT-BYF-1200 and DM-BYF-1300 cement pastes

Thermogravimetric analysis coupled with DSC (TGA-DSC) was used to complement the results obtained by XRPD in HT-BYF-1200 and DM-BYF-1300 cement pastes during the hydration process and to calculate the amount of chemically bounded water, to indirectly calculate the amount of free water. Before analysis, each sample was crushed and the hydration was stopped as detailed in the experimental section. TGA-DSC curves of both paste samples at different hardening ages are shown in Figures 7 and 8. Three mass losses accompanied by three endothermic peaks were observed. A doublet peak, detected between 50 and 150°C, corresponds to the dehydration of C-S-H and ettringite (AFt) [10,42,43]. Another peak was attributed to amorphous/nanocrystalline aluminum hydroxide (AH_3), which lost its bonded water in the temperature range 240-270°C [44]. AH_3 is not detected in XRPD patterns due to its small particle size [30,45,46]. The ettringite formation was very rapid and high amounts were formed after 1 day for both cements (Figures 7 and 8). Beyond 1 day, the ettringite amount in both cement pastes (HT-BYF-1200 and DM-BYF-1300) moderately increased with the hardening time which is in agreement with XRPD results. Gibbsite (AH_3) content was lower than ettringite (AFt) and its evolution appears slow with the hardening time for both cement pastes, as is shown in TGA curves (Figures 7 and 8). The amount of hydration products of HT-BYF-1200 cement paste were higher than DM-BYF-1300 during all hardening ages.

To complete TGA-DSC study and visualize the evolution of cement hydration, great amounts (3 g) of samples of HT-BYF-1200 and DM-BYF-1300 pastes of different hardening age were prepared for heating in furnace equipped with balance to measure the variation of mass loss in the temperature ranges of mineral transformation according to the TGA analysis. The studied loss mass concerns the evaporation of free water between 20 and 50°C, followed by the dehydration of ettringite and C-S-H at 80-180°C, and the dehydration of gibbsite between 200 and 300°C. The mass loss evolution of free water and bonded water of hydrates (ettringite, C-S-H and gibbsite mass losses) in both cement pastes were illustrated in Figure 9.

It was observed an important decrease of free water amount after 1 day of hardening for HT-BYF-1200 cement paste, accompanied by a great production of hydrates (ettringite, C-S-H, gibbsite) which was higher than for DM-BYF-1300 cement paste (Figure 9). After 1 day, the decrease of free water amount and the production of hydrates along hardening remain slower, especially for DM-BYF-1300 cement paste. These results are in agreement with XRPD ones and confirm the highest hydraulic reactivity of HT-BYF-1200 cement compared to DM-BYF-1300, which was due to the hydrothermal treatment of its raw mixture.

3.4.3. Study of synthesized cement hydration by Isothermal conduction calorimetry

To investigate the hydration behavior of both cements (HT-BYF-1200 and DM-BYF-1300) at very early age, isothermal conduction calorimetry technique was used. This technique measures the heat release of cement pastes as the hydration reactions of cement minerals are exothermics. The heat evolution rate of the synthesized cements is shown in Figure 10. The shape of the heat curves of both cements was similar (Figure 10-a). A single intense peak apeared 5 minutes after initiating hydration and was attributed to the initial formation of ettringite by rapid dissolution of ye'elimite in water. HT-BYF-1200 showed a high heat release compared to DM-BYF-1300. A large peak runing between 1 and 9 hours and acheiving its maximum after 2.5 h of hydration of HT-BYF-1200 cement, was attribued to the hydration reaction of mayenite and anhydrite producing more amounts of ettringite and gibbsite. This peak was practically non-existent in the case of DM-BYF-1300 cement, which shows that it is devoid of mayanite and its hydraulic reactivity is lower than HT-BYF-1200 cement. As it is shown by the accumulated hydration heat curves (Figure 10-b), the total heat release of HT-BYF-1200 (200 J/g) is higher than that of DM-BYF-1300 (125 J/g). The analysis results confirm the high hydraulic reactivity of both cements conducing to a rapid hardening, of which HT-BYF-1200 was higher.

3.5. Scanning electronic microscopy study of the synthesized clinkers and their pastes

Scanning electronic microscopy (SEM) was used to study the mineral morphology, texture and microporosity of the synthesized clinkers (HT-BYF-1200 and DM-BYF-1300) and their cement pastes. The various SEM observations are shown by micrographs of Figures 11, 12.

According to SEM observation, HT-BYF-1200 clinker appears less compact than DM-BYF-1300 clinker (Figure 11), which was in agreement with BET analysis giving 957.5 m^2/kg for HT-BYF-1200 and 716.3 m^2/kg for the second (Table 7). This is due to the vitreous phase which was less present in HT-BYF-1200 (Tables 8, 9), and leads to easy grinding of this clinker, as reported by other researchers [36,47,48]. Ye'elimite ($C_4A_3\check{S}$) particles appear as polygonal and tabular crystals (Figure 11).

Figure 12 shows SEM micrographs of both cement pastes (HT-BYF-1200, DM-BYF-1300) prepared with w/c equal to 0.5 and hardened for 3 and 14 days. The hydration products of both hardened samples are quite similar. A large amount of needle-like ettringite phases was observed which confirms the XRPD results showing that the main crystalline hydrated product was ettringite [45,49,50]. The ettringite amount in HT-BYF-1200 cement paste appears higher than that in DM-BYF-1300. The AFt phase formed in HT-BYF-1200 cement

paste was characterized by crystal form slightly longer and finer than that of DM-BYF-1300. These findings show that $C_4A_3\check{S}$ phases were fully hydrated after 3 days of hardening and moderate amount of amorphous gibbsite was produced with ettringite. This confirms that HT-BYF-1200 cement was very reactive than DM-BYF-1300, which conduces to high mechanical performances.

3.6. Compressive strength evolution of the synthesized cement mortars

The compressive strength tests were carried out on standard mortar specimens (4x4x16 cm^3) at room temperature with water/cement ratio of 0.5 and sand/cement ratio of 3:1, according to EN-196-1 standard. The compressive strength results of mortars of the synthesized cements (HT-BYF-1200, DM-BYF-1300) and the control cement (CEM I 42.5) at different hardening ages (2, 7 and 28 days) are reported in Figure 13. The compressive strength of cement mortars evolves with hardening time to achieve high values after 28 days, especially for HT-BYF-1200 recording a value (42.8 MPa) close to that of PC. The compressive strength of HT-BYF-1200 mortar begins low at early age (2 days of hardening), compared to DM-BYF-1300 and control mortars, despite the rapid hydration of this cement as deduced from XRPD and thermal analysis results. This was due to the rapid formation of ettringite after 1 day of hardening giving high amount of this expansive compound (Table 8) causing many cracks within cement matrix [11,51] as shown in Figure 13. A self repair of the mortar matrix with cracks sealing due to the crystallization of ettringite and the production of C-S-H resulting from β-C_2S hydration, were able to catch up the development of resistance with hardening age of HT-BYF-1200 mortar [40,51-53] . DM-BYF-1300 cement mortar achieved high resistance at early hardening age (15 MPa at 2 days) (Figure 13), due to the low ettringite content compared to HT-BYF-1200 (Tables 8, 9), avoiding the excessive formation of cracks within the mortar matrix. However, its evolution over time remains slower than HT-BYF-1200 mortar (Figure 13) because of the lower β-C_2S reactivity leading to less rapid hydration compared to that in the HT-BYF-1200 cement. The high hydration rate of β-C_2S in HT-BYF-1200 cement compared to DM-BYF-1300 is due to the hydrothermal treatment of raw mixture leading to the formation of belite phase at low temperature, which improves its chemical reactivity [27,28].

The mechanical test results showed that the obtained rich-sulfoaluminate belite cements are characterized by high resistance closes to the Portland cement I 42.5. Their compressive strength values at 28 days of hardening, 35 MPa for DM-BYF-1300 and 42.8 MPa for HT-BYF-1200, allow classifying them in the category of CEM I 32.5 and CEM I 42.5 cement

class, respectively. The high resistance value of HT-BYF-1200 mortar shows that the hydrothermal method allowed obtaining a clinker at low temperature with better mineralogical properties favorable for improving the mechanical performance of BYF cement.

4. Conclusion

An eco-binder of sulfoaluminate belite cement (BYF) was produced at low temperature, 1200ºC, from a mixture of industrial wastes and natural materials. This BYF cement is characterized by high mechanical performance, developing over 42 MPa of compressive strengths at 28 days of hydration, close to that of PC of class CEM I 42.5, which permits it to be used in all civil engineering applications.

The valorization of polluting by-products (hydraulic dam sludge, slaked lime dust and iron compound) to prepare a cement raw mixture of low carbonates and the low clinkering temperature of BYF cement, leading to reduce the CO_2 emissions, allow to consider it as ecological energy-saving binder. The low burning temperature (1200°C) results from the hydrothermal method used for the treatment of raw mixture of the BYF cement. Its manufacture without treatment conduces to increase its burning temperature to at last 1300°C.

The important mechanical resistance of this BYF cement is resulting from:

- The mineralogical composition, determined by XRPD, showing important amounts of $C_4A_3Š$, C_4AF and $C_{12}A_7$ phases, known by their rapid hydration. These allows to a rapid development of resistance due to the rapid formation of high amounts of ettringite, gibbsite, C-S-H which was shown by XRPD, SEM and thermal analysis.
- The higher surface specific area of BYF cement, which is a consequence of the hydrothermal treatment yielding to a clinker easier to be grinded, and consequently, conducing to a rapid hydration and hardening.
- The compact texture of BYF cement pastes with longs and fines crystals of ettringite, shown by SEM observation, leading to the reinforcement and consolidation of hydrated pastes.

Acknowledgements

This research is part of Ms. Bouha PhD. The authors would like to thank Spanish Junta de Andalucía for UMA18-FEDERJA-095 & P18-RT-720 research projects, which are cofounded by ERDF that funded Ms. Bouha stay at Universidad de Málaga (Spain). The authors also thank the Laboratory of Functional and Nano-structural Eco-material, USTO-MB, Algeria,

for their technical and scientific assistances. Authors acknowledge Lafarge Group Company in Algeria with its plant “Lafarge Ciment Oggaz (LCO)” for their material assistance.

References

[1] J.G.J. Olivier, G. Janssens-Maenhout, M. Muntean, J. Peters, Trends in Global CO2 Emissions: 2016 Report;PBL Netherlands Environmental Assessment Agency: The Hague, PBL Netherlands Environ. Assess. Agency Eur. Comm. Jt. Res. Cent. (2016) 86.

[2] T. Hanein, T.Y. Duvallet, R.B. Jewell, A.E. Oberlink, T.L. Robl, Y. Zhou, F.P. Glasser, M.N. Bannerman, Alite calcium sulfoaluminate cement: Chemistry and thermodynamics, Adv. Cem. Res. 31 (2019) 94–105. https://doi.org/10.1680/jadcr.18.00118.

[3] K.H. Yang, Y.B. Jung, M.S. Cho, S.H. Tae, Effect of supplementary cementitious materials on reduction of CO2 emissions from concrete, J. Clean. Prod. 103 (2015) 774–783. https://doi.org/10.1016/j.jclepro.2014.03.018.

[4] E. Crossin, The greenhouse gas implications of using ground granulated blast furnace slag as a cement substitute, J. Clean. Prod. 95 (2015) 101–108. https://doi.org/10.1016/j.jclepro.2015.02.082.

[5] E. Gartner, T. Sui, Alternative cement clinkers, Cem. Concr. Res. (2017). https://doi.org/10.1016/j.cemconres.2017.02.002.

[6] E. Gartner, Industrially interesting approaches to “low-CO2” cements, Cem. Concr. Res. 34 (2004) 1489–1498. https://doi.org/10.1016/j.cemconres.2004.01.021.

[7] K.L. Scrivener, V.M. John, E.M. Gartner, Eco-efficient cements: Potential economically viable solutions for a low-CO2 cement-based materials industry, Cem. Concr. Res. 114 (2018) 2–26. https://doi.org/10.1016/j.cemconres.2018.03.015.

[8] G.Á. Pinazo, Active sulpho-belite cements. Hydration mechanisms and mechanical, The University of Malaga Dissertation (PhD.), 2015.

[9] M.A.G. Aranda, A.G. De la Torre, Sulfoaluminate cement, in: Eco-Efficient Concr., 2013: pp. 488–522. https://doi.org/10.1533/9780857098993.4.488.

[10] D. Londono-Zuluaga, J.I. Tobón, M.A.G. Aranda, I. Santacruz, A.G. De la Torre, Clinkering and hydration of belite-alite-ye´elimite cement, Cem. Concr. Compos. 80 (2017) 333–341. https://doi.org/10.1016/j.cemconcomp.2017.04.002.

[11] L. Senff, a Castela, W. Hajjaji, D. Hotza, J. a Labrincha, Formulations of sulfobelite cement through design of experiments, Constr. Build. Mater. 25 (2011) 3410–3416. https://doi.org/10.1016/j.conbuildmat.2011.03.032.

[12] A.J.M. Cuberos, A.G. De la Torre, G. Alvarez-Pinazo, M.C. Martín-Sedeño, K. Schollbach, H. Pöllmann, M.A.G. Aranda, G. Álvarez-Pinazo, Active iron-rich belite sulfoaluminate cements: Clinkering and hydration, Environ. Sci. Technol. 44 (2010) 6855–6862.

[13] E.A. El-Alfi, R.A. Gado, Preparation of calcium sulfoaluminate-belite cement from

marble sludge waste, Constr. Build. Mater. 113 (2016) 764–772. https://doi.org/10.1016/j.conbuildmat.2016.03.103.

[14] A. Klein, Calcium aluminosulfate and expansive cement containing same, 1963. https://doi.org/10.1145/178951.178972.

[15] A. Klein, G.E. Troxell, Studies of calcium sulfoalurninate admixtures for expansive cements, in: Proc. Am. Soc. Test. Mater., ASTM, 1958: pp. 986–1008.

[16] F.P. Glasser, L. Zhang, High-performance cement matrices based on calcium sulfoaluminate-belite compositions, Cem. Concr. Res. 31 (2001) 1881–1886. https://doi.org/10.1016/S0008-8846(01)00649-4.

[17] G. Álvarez-Pinazo, I. Santacruz, L. León-Reina, M.A.G. Aranda, A.G. De La Torre, Hydration reactions and mechanical strength developments of iron-rich sulfobelite eco-cements, Ind. Eng. Chem. Res. 52 (2013) 16606–16614. https://doi.org/10.1021/ie402484e.

[18] V. Morin, G. Walenta, E. Gartner, P. Termkhajornkit, I. Baco, J.M. Casabonne, Hydration of a Belite-Calcium Sulfoaluminate-Ferrite cement : Aether TM, 13th Int. Congr. Chem. Cem. (2011) 1–7.

[19] Á.G. De La Torre, A.J.M. Cuberos, G. Álvarez-Pinazo, A. Cuesta, M.A.G. Aranda, In situ powder diffraction study of belite sulfoaluminate clinkering, J. Synchrotron Radiat. 18 (2011) 506–514. https://doi.org/10.1107/S0909049511005796.

[20] P. Arjunan, M.R. Silsbee, D.M. Roy, Sulfoaluminate-belite cement from low-calcium fly ash and sulfur-rich and other industrial by-products, Cem. Concr. Res. 29 (1999) 1305–1311. https://doi.org/10.1016/S0008-8846(99)00072-1.

[21] I.A. Chen, M.C.G. Juenger, Incorporation of coal combustion residuals into calcium sulfoaluminate-belite cement clinkers, Cem. Concr. Compos. 34 (2012) 893–902. https://doi.org/10.1016/j.cemconcomp.2012.04.006.

[22] V. Isteri, K. Ohenoja, T. Hanein, H. Kinoshita, P. Tanskanen, M. Illikainen, T. Fabritius, Production and properties of ferrite-rich CSAB cement from metallurgical industry residues, Sci. Total Environ. 712 (2020) 136208. https://doi.org/10.1016/j.scitotenv.2019.136208.

[23] E.B. da Costa, E.D. Rodríguez, S.A. Bernal, J.L. Provis, L.A. Gobbo, A.P. Kirchheim, Production and hydration of calcium sulfoaluminate-belite cements derived from aluminium anodising sludge, Constr. Build. Mater. 122 (2016) 373–383. https://doi.org/10.1016/j.conbuildmat.2016.06.022.

[24] K. Byrappa, T. Adschiri, Hydrothermal technology for nanotechnology, Prog. Cryst. Growth Charact. Mater. 53 (2007) 117–166. https://doi.org/10.1016/j.pcrysgrow.2007.04.001.

[25] H. Ishida, K. Mabuchi, K. Sasaki, Low-Temperature Synthesis of β-Ca2SiO4, from, from Hillebrandite, (1992).

[26] K. Pimraksa, S. Hanjitsuwan, P. Chindaprasirt, Synthesis of belite cement from lignite fly ash, 35 (2009) 2415–2425. https://doi.org/10.1016/j.ceramint.2009.02.006.

[27] L. Kacimi, M. Cyr, P. Clastres, Synthesis of α'L-C2S cement from fly-ash using the hydrothermal method at low temperature and atmospheric pressure, J. Hazard. Mater. 181 (2010) 593–601. https://doi.org/10.1016/j.jhazmat.2010.05.054.

[28] W. Mazouzi, L. Kacimi, M. Cyr, P. Clastres, Cement & Concrete Composites Properties of low temperature belite cements made from aluminosilicate wastes by hydrothermal method, Cem. Concr. Compos. 53 (2014) 170–177. https://doi.org/10.1016/j.cemconcomp.2014.07.001.

[29] A. Rungchet, P. Chindaprasirt, S. Wansom, K. Pimraksa, Hydrothermal synthesis of calcium sulfoaluminate-belite cement from industrial waste materials, J. Clean. Prod. 115 (2016) 273–283. https://doi.org/10.1016/j.jclepro.2015.12.068.

[30] F. Winnefeld, B. Lothenbach, Hydration of calcium sulfoaluminate cements - Experimental findings and thermodynamic modelling, Cem. Concr. Res. 40 (2010) 1239–1247. https://doi.org/10.1016/j.cemconres.2009.08.014.

[31] M.C.G. Juenger, F. Winnefeld, J.L. Provis, J.H. Ideker, Advances in alternative cementitious binders, Cem. Concr. Res. 41 (2011) 1232–1243. https://doi.org/10.1016/j.cemconres.2010.11.012.

[32] C.W. Hargis, A.P. Kirchheim, P.J.M. Monteiro, E.M. Gartner, Early age hydration of calcium sulfoaluminate (synthetic ye'elimite, C 4A3S̄) in the presence of gypsum and varying amounts of calcium hydroxide, Cem. Concr. Res. 48 (2013) 105–115. https://doi.org/10.1016/j.cemconres.2013.03.001.

[33] M. García-Maté, A.G. De La Torre, L. León-Reina, E.R. Losilla, M.A.G. Aranda, I. Santacruz, Effect of calcium sulfate source on the hydration of calcium sulfoaluminate eco-cement, Cem. Concr. Compos. 55 (2015) 53–61. https://doi.org/10.1016/j.cemconcomp.2014.08.003.

[34] A.G. De la Torre, S. Bruque, M.A.G. Aranda, Rietveld quantitative amorphous content analysis, J. Appl. Crystallogr. 34 (2001) 196–202. https://doi.org/10.1107/S0021889801002485.

[35] M.A.G. Aranda, A. Cuesta, A.G. De la Torre, I. Santacruz, L. León-Reina, Diffraction and crystallography applied to hydrating cements, 2017. https://doi.org/10.1515/9783110473728-003.

[36] M.C. Martín-Sedeño, A.J.M. Cuberos, A.G. De la Torre, G. Álvarez-Pinazo, L.M. Ordónez, M. Gateshki, M.A.G. Aranda, Aluminum-rich belite sulfoaluminate cements: Clinkering and early age hydration, Cem. Concr. Res. 40 (2010) 359–369. https://doi.org/10.1016/j.cemconres.2009.11.003.

[37] E. Gartner, H. Hirao, A review of alternative approaches to the reduction of CO2 emissions associated with the manufacture of the binder phase in concrete, Cem. Concr. Res. 78 (2015) 126–142. https://doi.org/10.1016/j.cemconres.2015.04.012.

[38] K.L. Scrivener, V.M. John, E.M. Gartner, Eco-efficient cements: Potential economically viable solutions for a low-CO2 cement-based materials industry, Cem. Concr. Res. 114 (2018) 2–26. https://doi.org/10.1016/j.cemconres.2018.03.015.

[39] A. Cuesta, A.G. De la Torre, I. Santacruz, P. Trtik, J.C. da Silva, A. Diaz, M. Holler, M.A.G. Aranda, Chemistry and Mass Density of Aluminum Hydroxide Gel in Eco-

Cements by Ptychographic X-ray Computed Tomography, J. Phys. Chem. C. 121 (2017) 3044–3054. https://doi.org/10.1021/acs.jpcc.6b10048.

[40] V. Morin, P. Termkhajornkit, B. Huet, G. Pham, Impact of quantity of anhydrite, water to binder ratio, fineness on kinetics and phase assemblage of belite-ye'elimite-ferrite cement, Cem. Concr. Res. 99 (2017) 8–17. https://doi.org/10.1016/j.cemconres.2017.04.014.

[41] Y. Jeong, C.W. Hargis, S.C. Chun, J. Moon, The effect of water and gypsum content on strätlingite formation in calcium sulfoaluminate-belite cement pastes, Constr. Build. Mater. 166 (2018) 712–722. https://doi.org/10.1016/j.conbuildmat.2018.01.153.

[42] R. Trauchessec, J.M. Mechling, A. Lecomte, A. Roux, B. Le Rolland, Hydration of ordinary Portland cement and calcium sulfoaluminate cement blends, Cem. Concr. Compos. 56 (2015) 106–114. https://doi.org/10.1016/j.cemconcomp.2014.11.005.

[43] F. Winnefeld, S. Barlag, Calorimetric and thermogravimetric study on the influence of calcium sulfate on the hydration of ye'elimite, J. Therm. Anal. Calorim. 101 (2010) 949–957. https://doi.org/10.1007/s10973-009-0582-6.

[44] A. Telesca, M. Marroccoli, M.L. Pace, M. Tomasulo, G.L. Valenti, P.J.M. Monteiro, A hydration study of various calcium sulfoaluminate cements, Cem. Concr. Compos. 53 (2014) 224–232. https://doi.org/10.1016/j.cemconcomp.2014.07.002.

[45] M. Zajac, J. Skocek, F. Bullerjahn, M. Ben Haha, Effect of retarders on the early hydration of calcium-sulpho-aluminate (CSA) type cements, Cem. Concr. Res. 84 (2016) 62–75. https://doi.org/10.1016/j.cemconres.2016.02.014.

[46] L. Pelletier, F. Winnefeld, B. Lothenbach, The ternary system Portland cement-calcium sulphoaluminate clinker-anhydrite: Hydration mechanism and mortar properties, Cem. Concr. Compos. 32 (2010) 497–507. https://doi.org/10.1016/j.cemconcomp.2010.03.010.

[47] I. Odler, H. Zhang, Investigations on high SO3 Portland clinkers and cements, Cem. Concr. Res. 66 (1996) 1307-1313,1315-1324.

[48] L. Kacimi, a. Simon-Masseron, a. Ghomari, Z. Derriche, Reduction of clinkerization temperature by using phosphogypsum, J. Hazard. Mater. 137 (2006) 129–137. https://doi.org/10.1016/j.jhazmat.2005.12.053.

[49] S. Ioannou, L. Reig, K. Paine, K. Quillin, Properties of a ternary calcium sulfoaluminate-calcium sulfate-fly ash cement, Cem. Concr. Res. 56 (2014) 75–83. https://doi.org/10.1016/j.cemconres.2013.09.015.

[50] J. Zhang, X. Guan, X. Wang, X. Ma, Z. Li, Z. Xu, B. Jin, Microstructure and Properties of Sulfoaluminate Cement-Based Grouting Materials: Effect of Calcium Sulfate Variety, Adv. Mater. Sci. Eng. 2020 (2020). https://doi.org/10.1155/2020/7564108.

[51] D. Su, Q. Li, Y. Guo, G. Yue, L. Wang, Effect of residual CaSo4 in clinker on properties of high belite sulfoaluminate cement based on solid wastes, Materials (Basel). 13 (2020). https://doi.org/10.3390/ma13020429.

[52] J. Bizzozero, C. Gosselin, K.L. Scrivener, Expansion mechanisms in calcium aluminate and sulfoaluminate systems with calcium sulfate, Cem. Concr. Res. 56 (2014) 190–

202. https://doi.org/10.1016/j.cemconres.2013.11.011.

[53] I.A. Chen, C.W. Hargis, M.C.G. Juenger, Understanding expansion in calcium sulfoaluminate-belite cements, Cem. Concr. Res. 42 (2012) 51–60. https://doi.org/10.1016/j.cemconres.2011.07.010.

Table captions

Figure captions

Tables

Table1. Chemical composition, expressed as oxides in weight percentage (wt%), of raw materials

Oxides	**Sludge (SLD)**	**Gypsum (GS)**	**Lime Dust (LD)**	**Iron ore (IO)**	**Pure Alumina (PA)**
CaO	14.5	33.8	72	0.3	-
SiO_2	45.1	2.7	1.5	0.8	-
Al_2O_3	13.6	0.9	0.7	1.2	99.4
Fe_2O_3	6.1	0.2	0.3	80.6	-
SO_3	0.2	43.9	0.2	1.5	-
MgO	3	0.4	0.7	0.3	-
K_2O	3.3	0.2	0.1	0.3	-
Na_2O	0.1	-	0.1	0.6	-
P_2O_5	0.1	-	-	-	-
ZnO	-	-	-	1.8	-
TiO_2	0.6	-	0.1	0.1	-
LOI*	13.3	17.8	24.3	2.3	0.6

(*) LOI: Loss Of Ignition

Table 2. Chemical formula and ICSD codes of mineral phases of the studied materials

Mineral phase	**Cementitious symbol**	**Chemical formula**	**ICSD Code**
Belite	β-C_2S	Ca_2SiO_4	81096
Cub-Ye'elimite	C-$C_4A_3Š$	$Ca_4Al_6O_{12}SO_4$	9560
Ortho-Ye'elimite	O-$C_4A_3Š$	$Ca_4Al_6O_{12}SO_4$	80361
Brownmillerite	C_4AF	$Fe_2O_3Al_2O_3(CaO)_4$	009197
Mayenite	$C_{12}A_7$	$12CaO.7Al_2O_3$	241243
Anhydrite	CŠ	$CaSO_4$	1956
Ettringite	AFt	$Ca_6Al_2\ (SO4)_3(OH)_{12}\cdot 26H_2O$	155395
Magnesia	M	MgO	009853
Calcite	CĈ	$CaCO_3$	80869
Quartz	S	SiO_2	90145
Muscovite $2M_1$	Mu	$KAl_2(Si_3Al)O_{10}(OH)_2$	34353
Gypsum	$CŠH_2$	$CaSO_4\cdot 2H_2O$	081650
Portlandite	CH	$Ca(OH)_2$	73468
Kuzelite	$C_4AŠH_{12}$	$(Ca_2Al(OH)_6)(S_{0.5}O_2(OH_2)_3)$	100138
Corundum	A	Al_2O_3	60419
Dolomite	$CMĈ_2$	$CaMg(CO_3)_2$	40970
Hematite	F	Fe_2O_3	022505

Table 3. Dosification of raw materials to produce BYF clinkers

Raw materials	**Sludge (SLD)**	**Lime Duste (LD)**	**Gypsum (GS)**	**Pure Alumina (PA)**	**Iron ore (IO)**
Mass percentage (wt%)	33.1	46.5	11.0	7.3	2.1

Table 4. Mineralogical composition (wt%) of HT and DM raw mixtures determined by Rietveld method

Mineral phases	**Mass composition (wt%) of mixtures**	
	HT	**DM**
Quartz	7.2(1)	6.3(2)
Calcite	15.5(7)	10.6(2)
Muscovite $2M_1$	5.0(3)	10.0(1)
Corundum	12.3(2)	7.1(3)
Gypsum	2.3(6)	4(1)
Portlandite	53.1(4)	60.1(4)
Kuzelite	3.7(1)	-
Hematite	0.9(5)	0.9(1)
Dolomite	1.0(2)	1.0(2)

Numbers between brackets are mathematical errors from Rietveld fits

Table 5. Mineralogical compositions (wt%), determined by Rietveld method (RQPA), of the synthesized clinkers (HT-BYF, DM-BYF) at different burning temperatures

Mineral phases	HT-BYF for different burning temperatures				DM-BYF-1300°C
	1100°C	1200°C	1250°C	1300°C	
β-C_2S	63.5(3)	56.6(3)	55.7(3)	55.2(3)	64.2(3)
c-$C_4A_3Š$	2.7(3)	4.5(3)	4.8(2)	5.3(3)	4.3(4)
o-$C_4A_3Š$	15.7(4)	19.7(4)	22.5(3)	22.8(4)	18.4(5)
C_4AF	10.8(2)	11.6(2)	12.0(2)	15.4(2)	11.2(2)
$C_{12}A_7$	5.9(1)	6.2(1)	3.7(1)	-	-
SiO_2	-	-	-	-	0.7(5)
MgO	1.4(8)	1.4(7)	1.3(7)	1.3(7)	1.2(7)

Numbers between brackets are mathematical errors from Rietveld fits

Table 6. Chemical composition (wt%) by XRF of HT-BYF-1200 and DM-BYF-1300 clinkers

Clinkers	Chemical composition (wt%)						
	CaO	**SiO_2**	**Al_2O_3**	**Fe_2O_3**	**SO_3**	**MgO**	**K_2O**
HT-BYF-1200	52.5	19	15.1	4.4	5.4	1.4	1.2
DM-BYF-1300	53.1	18.2	15.4	4.5	5.3	1.4	1.2

Table 7. Physical properties of the synthesized clinkers (HT-BYF-1200 and DM-BYF-1300)

Clinker	**Specific Surface Area BET method (m^2/kg)**	**Specific Surface Area Blaine method (m^2/kg)**	**Density (g/cm^3)**
HT-BYF 1200	957.5	364.5	3.1
DM-BYF-1300	716.3	292.6	3.1

Table 8. Mineralogical compositions (wt%), determined by RQPA Rietveld method, of HT-BYF-1200 cement paste after 0, 1, 3, 7, 14 and 28 days of hardening

Mineral	**Hardening time of HT-BYF-1200 cement paste (day)**					
phases	**0**	**1**	**3**	**7**	**14**	**28**
β-C_2S	28.9(2)	26.2(2)	24.1(3)	19.1(2)	15.3(2)	10.8(2)
c-$C_4A_3Š$	2.6(3)	-	-	-	-	-
o-$C_4A_3Š$	10.9(4)	-	-	-	-	-
C_4AF	4.0(1)	3.8(2)	3.5(2)	3.3(1)	3.2(2)	3.1(2)
$C_{12}A_7$	4.7(1)	1.4(1)	1.3(2)	1.3(8)	1(1)	0.9(1)
C Š	5.7(2)	1.3(6)	-	-	-	-
AFt	-	24.5(2)	27.4(3)	32.7(2)	36.4(2)	37.8(2)
MgO	0.8(6)	0.6(7)	0.6(1)	0.5(5)	0.4(7)	0.4(6)
ACn	9.2	27.1	30.7	32	33.4	36.9
FW	33.3	15.1	12.4	11.1	10.3	10

Numbers between brackets are mathematical errors from Rietveld fits

Table 9. Mineralogical compositions (wt%), determined by RQPA Rietveld method, of DM-BYF-1300 cement paste after 0, 1, 3, 7, 14 and 28 days of hardening

Mineral	**Hardening time of DM-BYF-1300 cement paste (day)**					
phases	**0**	**1**	**3**	**7**	**14**	**28**
β-C_2S	25.4(3)	24.3(2)	22.8(2)	21.7(3)	18.5(2)	16.8(3)
c-$C_4A_3Š$	1.1(4)	-	-	-	-	-
o-$C_4A_3Š$	7.4(5)	0.9(9)	-	-	-	-
C_4AF	4.6(1)	4.3(1)	3.6(1)	3.3(1)	2.7(1)	2.4(1)
CŠ	4.4(2)	1.1(8)	-	-	-	-
AFt	-	14.8(2)	20(2)	20.8(2)	23.3(2)	25.6(3)
MgO	0.3(7)	0.3(6)	0.3(6)	0.3(6)	0.3(6)	0.3(6)
ACn	23.4	34	35.2	36.9	39.4	40.9
FW	33.3	20.2	18	16.9	15.7	13.9

Numbers between brackets are mathematical errors from Rietveld fits

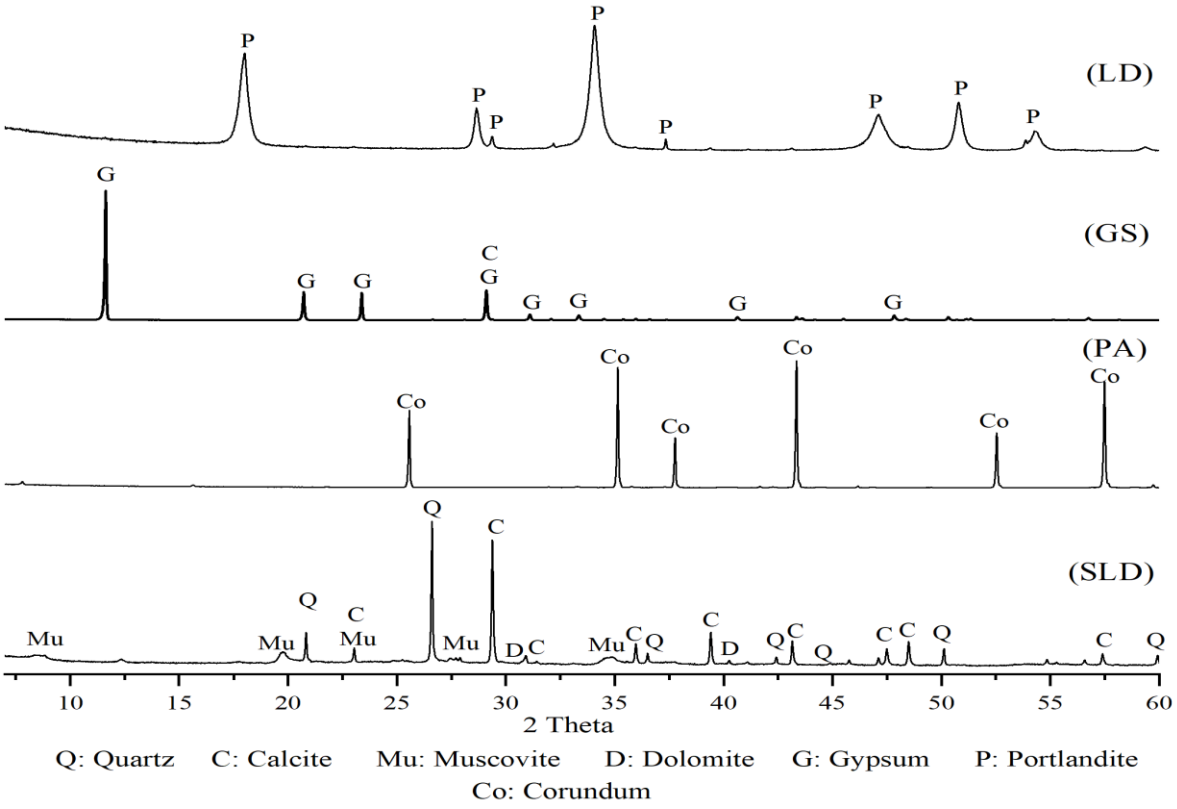

Figure 1. XRPD patterns of raw materials: Sludge (SLD), Pure Alumina (PA), Gypsum (GS) and Lime Dust (LD)

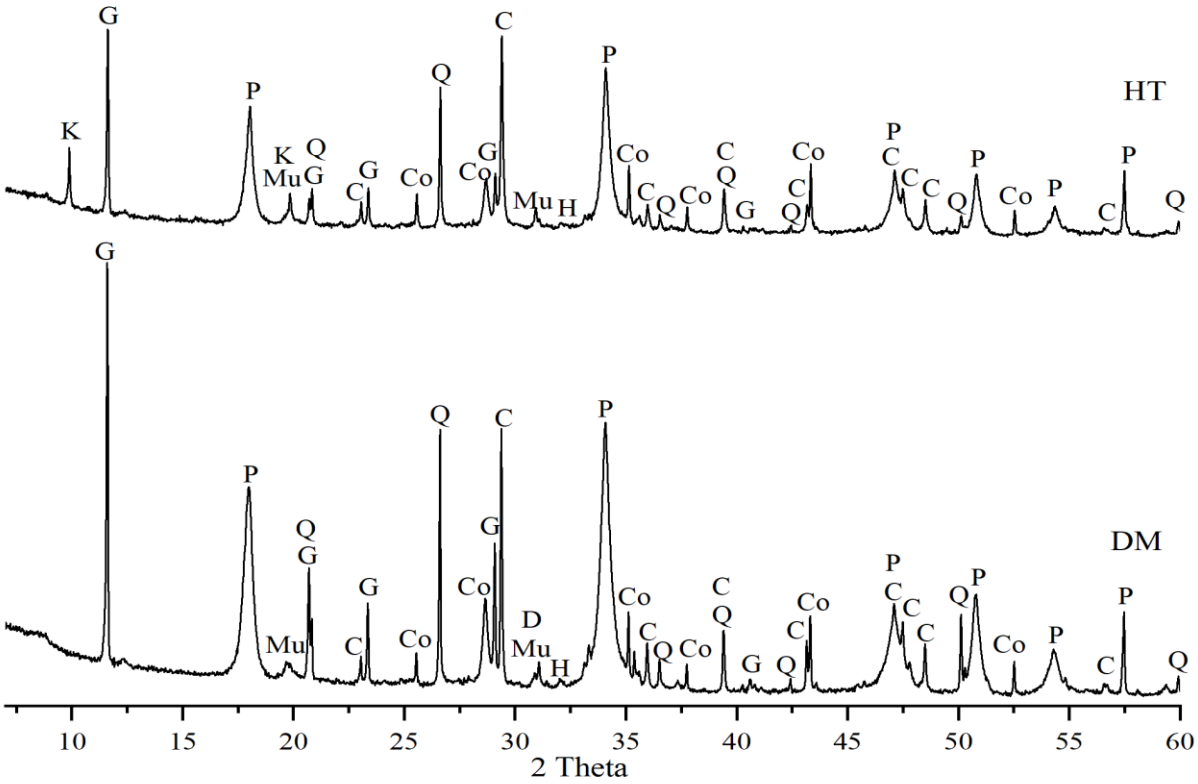

Figure 2. XRPD patterns of hydrothermal precursor (HT) and dry raw mixture (DM)

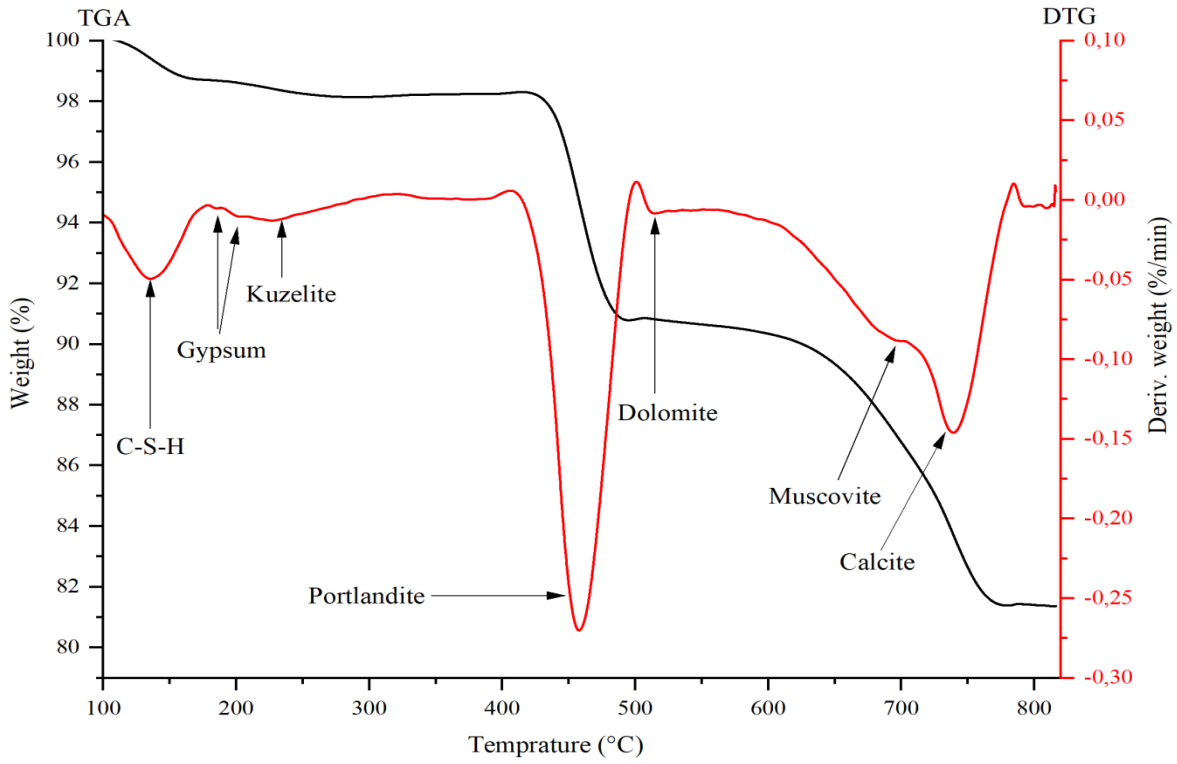

Figure 3. TGA-DTG curves of the hydrothermal precursor HT-BYF

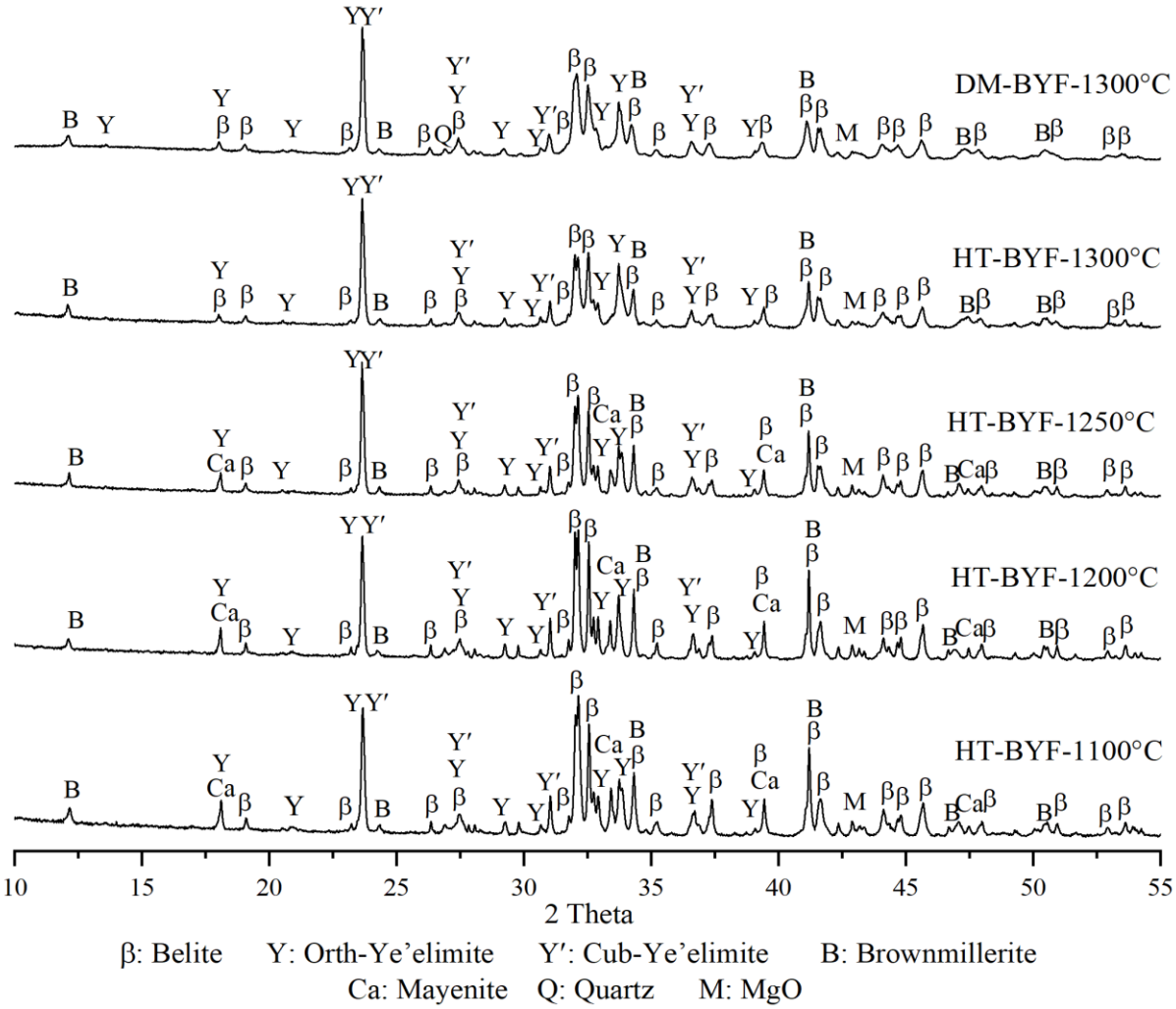

Figure 4. XRPD patterns of the synthesized clinkers of different treatment type and burning temperatures (1100, 1200, 1250 and 1300°C)

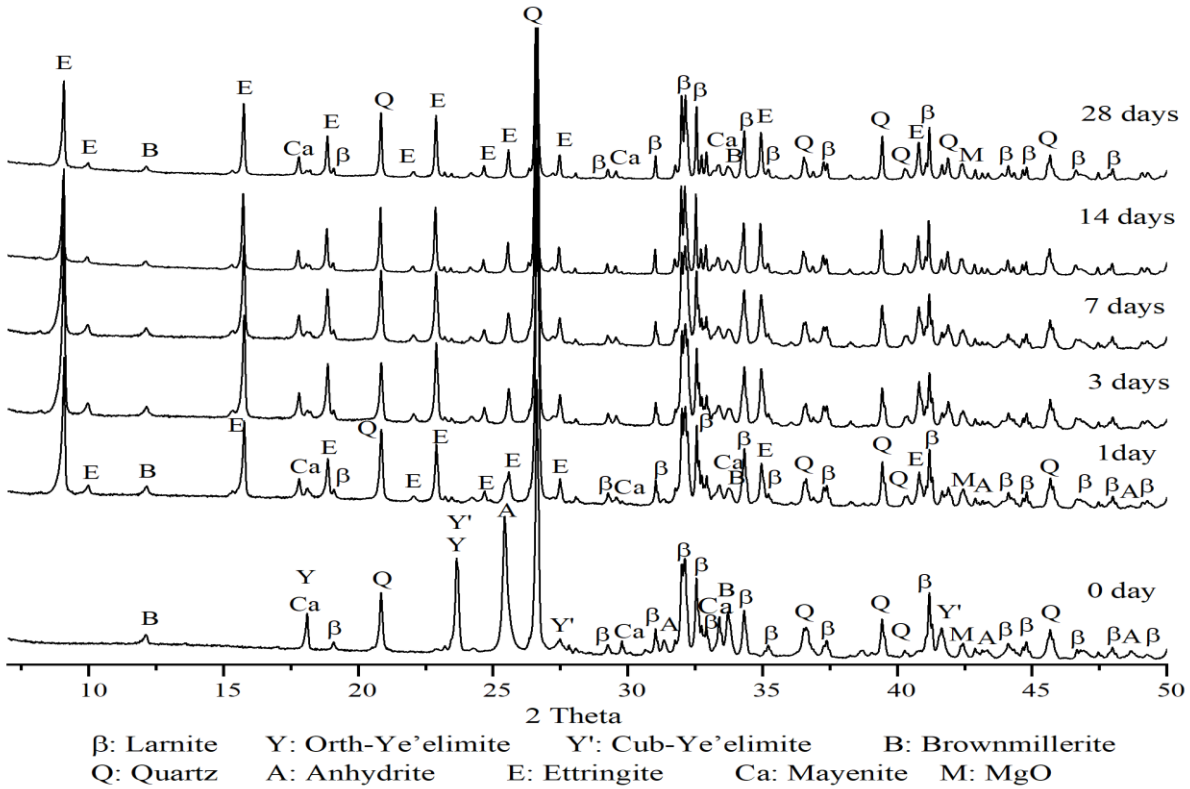

Figure 5. XRPD patterns of HT-BYF-1200 cement paste after 0, 1, 3, 7, 14 and 28 days of hardening

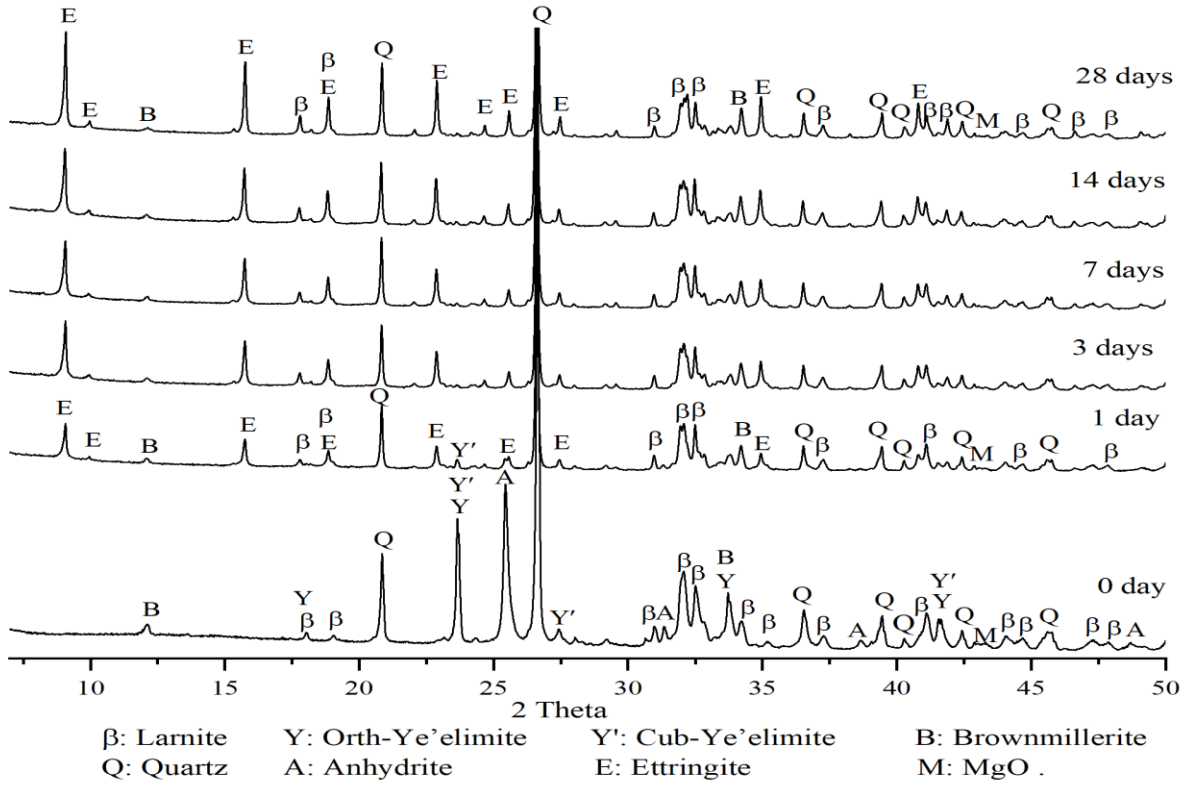

Figure 6. XRPD patterns of DM-BYF-1300 cement paste after 0, 1, 3, 7, 14 and 28 days of hardening

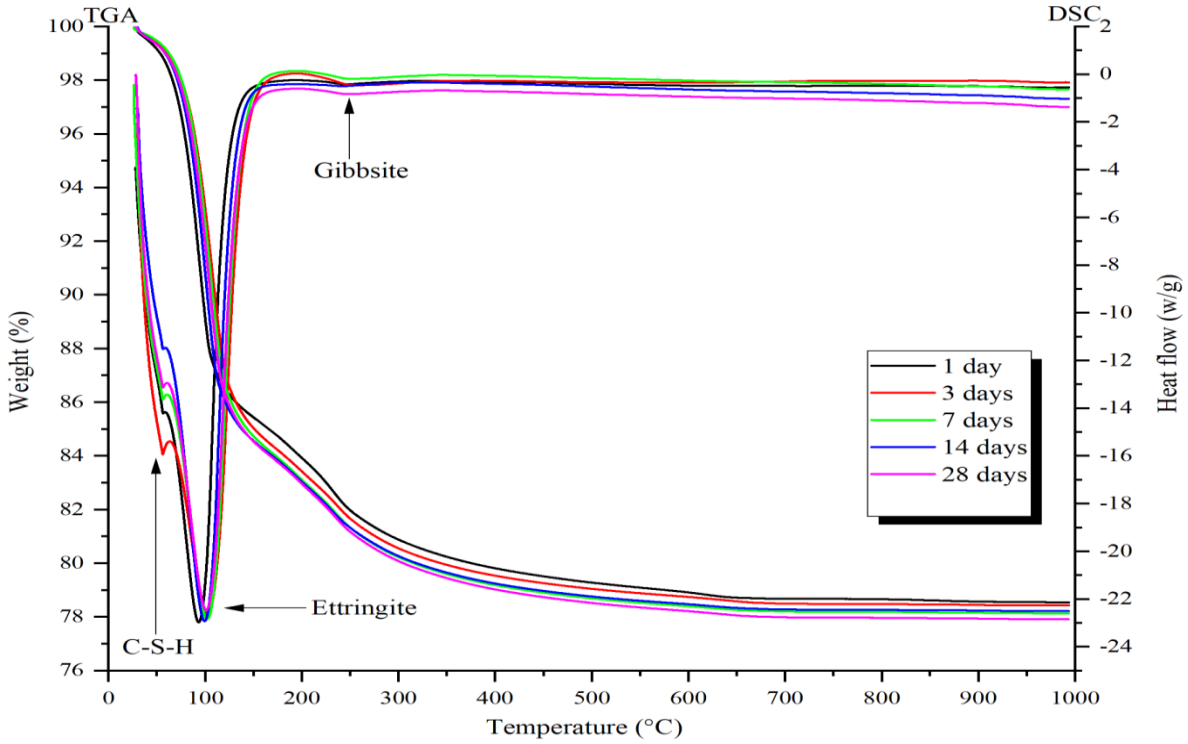

Figure 7. TGA/DSC curves of HT-BYF-1200 cement pastes at 1, 3, 7, 14 and 28 days of hardening

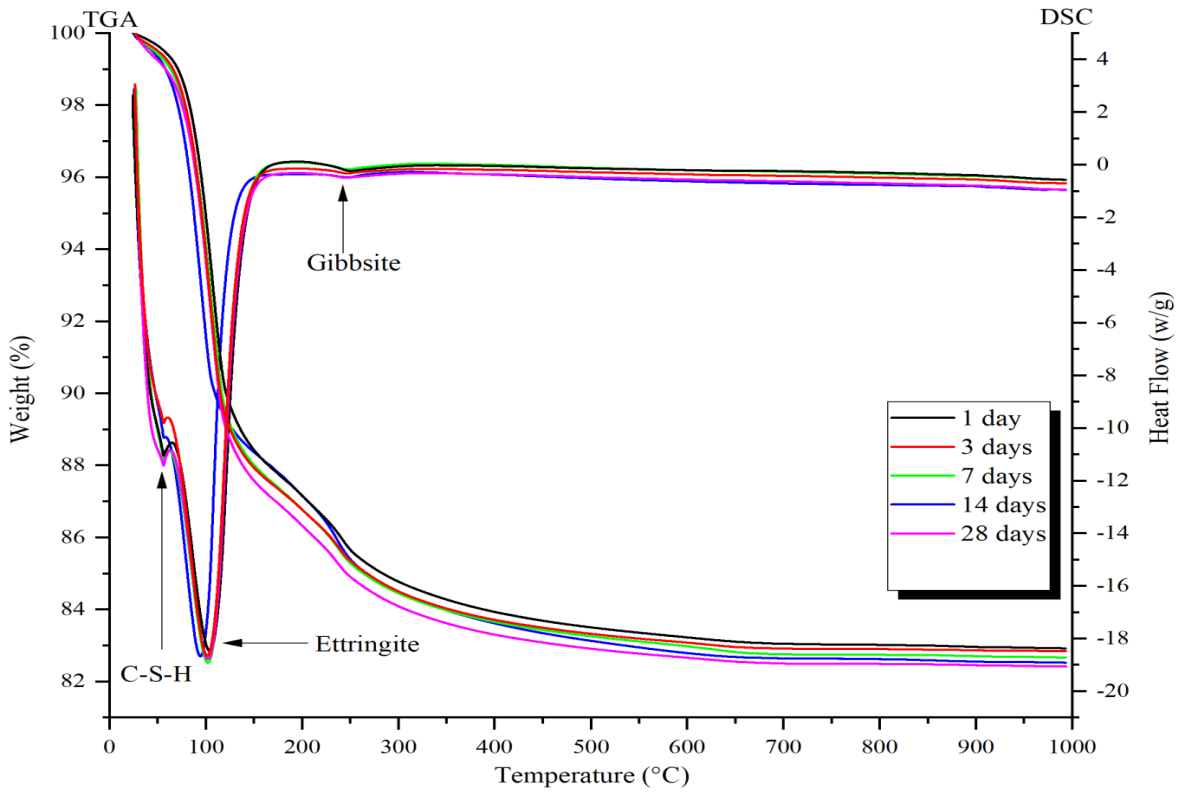

Figure 8. TGA-DSC curves of DM-BYF-1300 cement pastes at 1, 3, 7, 14 and 28 days of hardening

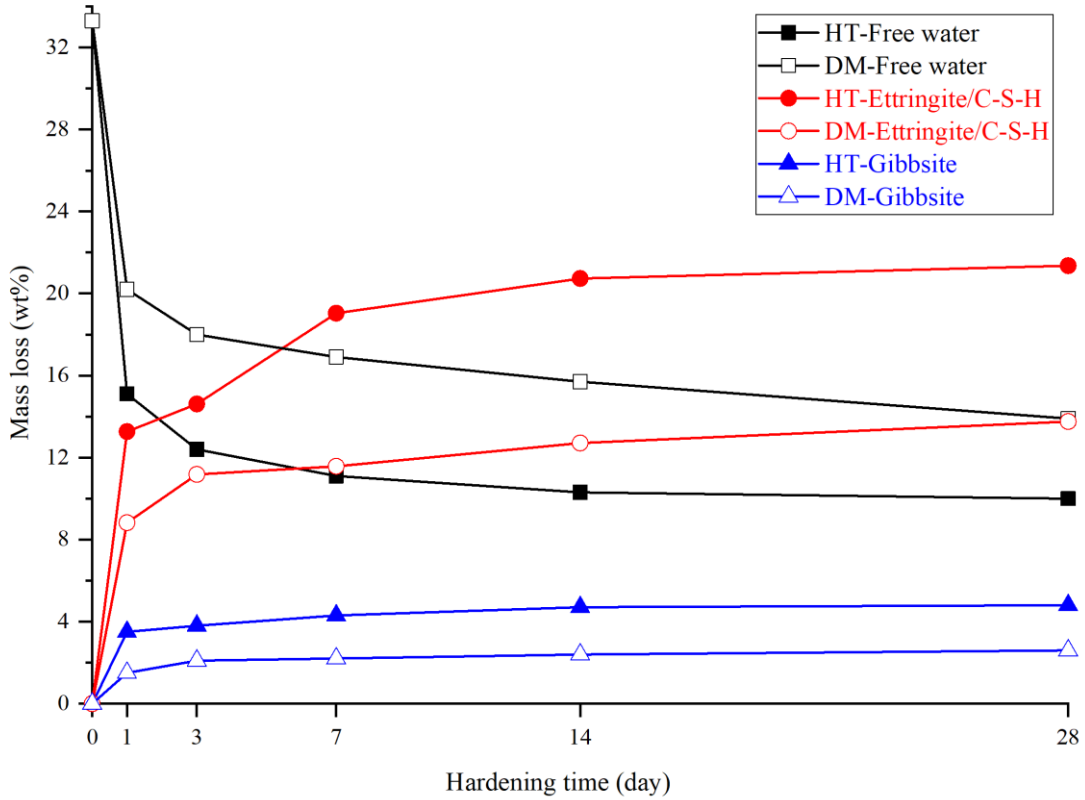

Figure 9. Mass loss (wt%) of free water, ettringite/C-S-H and gibbsite contained in HT-BYF-1200 and DM-BYF-1300 cement pastes with hardening age

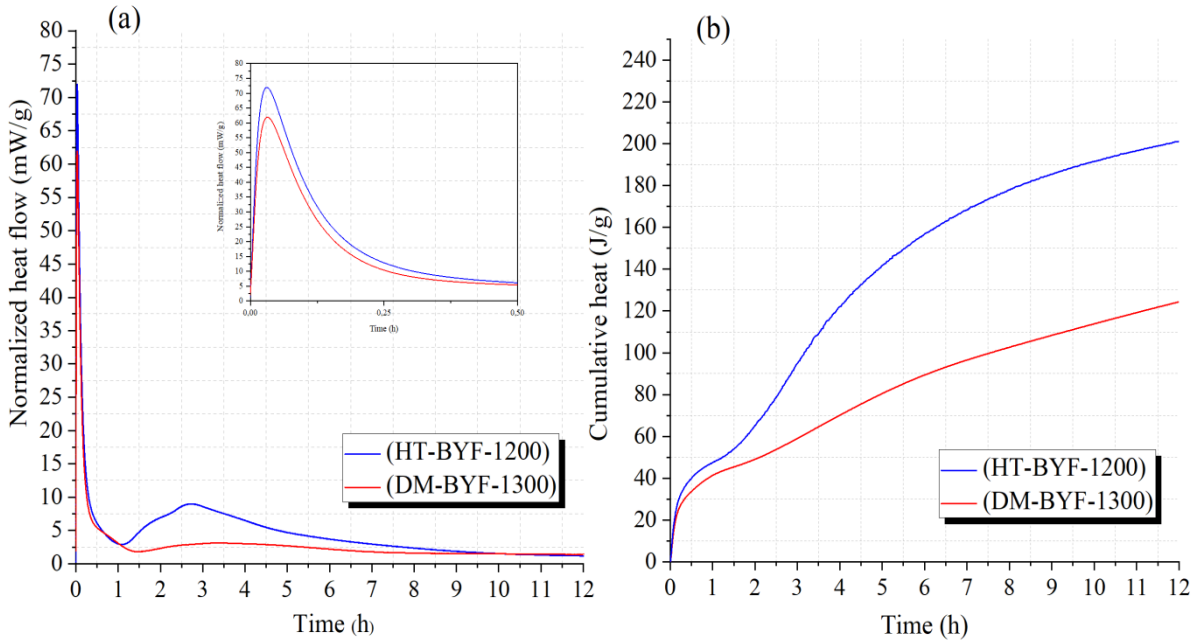

Figure 10. Calorimetric curves of HT-BYF-1200 and DM-BYF-1300 cement hydration

(a) Heat flow (b) Accumulated heat release

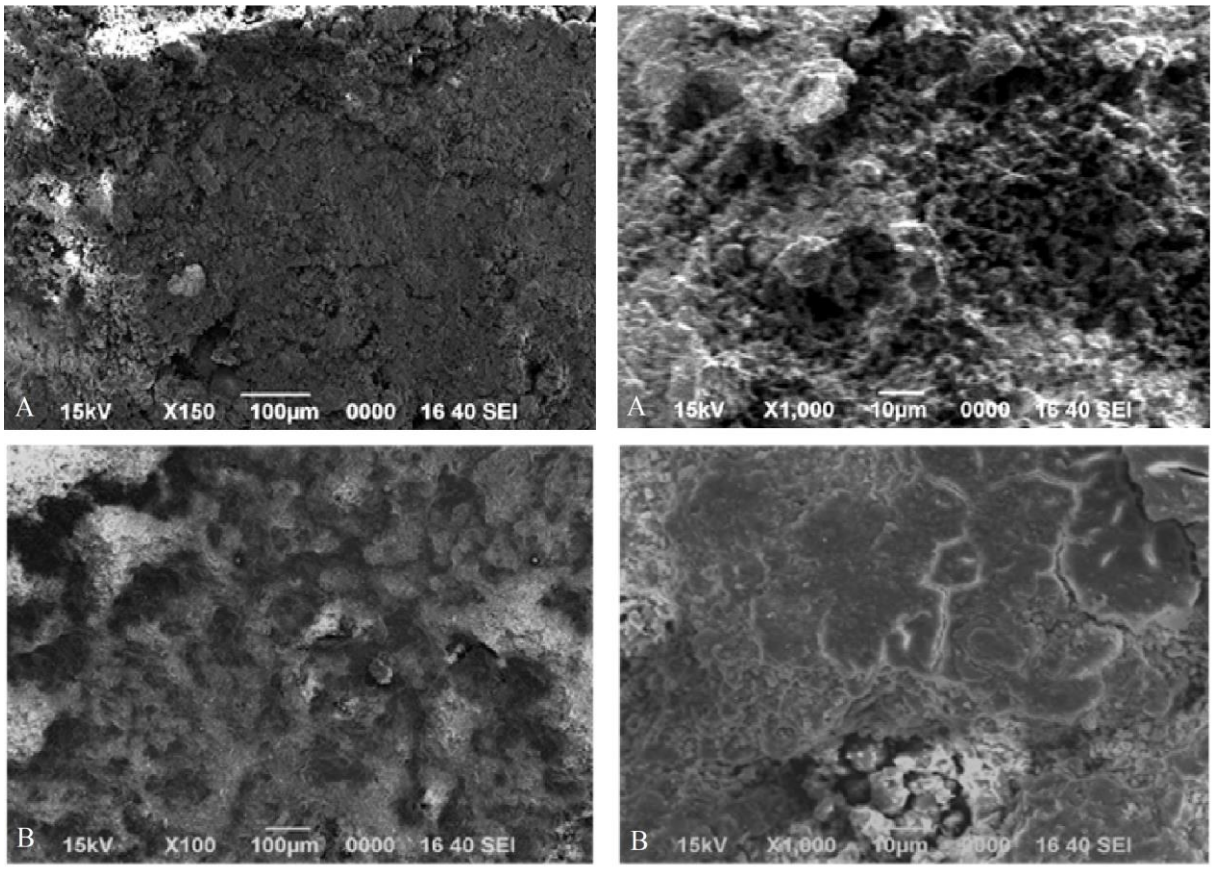

Figure 11. SEM micrographs of the synthesized clinkers

(A)HT-BYF-1200, (B) DM- BYF-1300

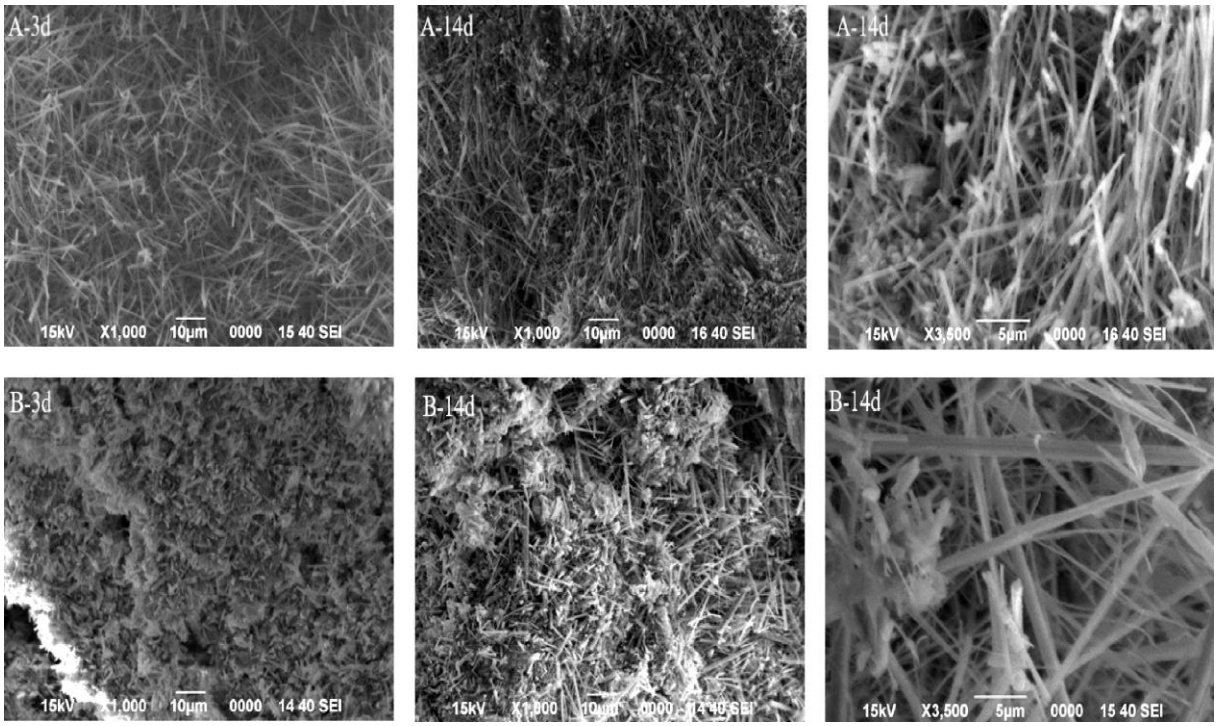

Figure 12. SEM micrographs of cement pastes after 3 and 14 days of hardening (A) HT-BYF-1200 cement paste, (B) DM-BYF-1300 cement paste

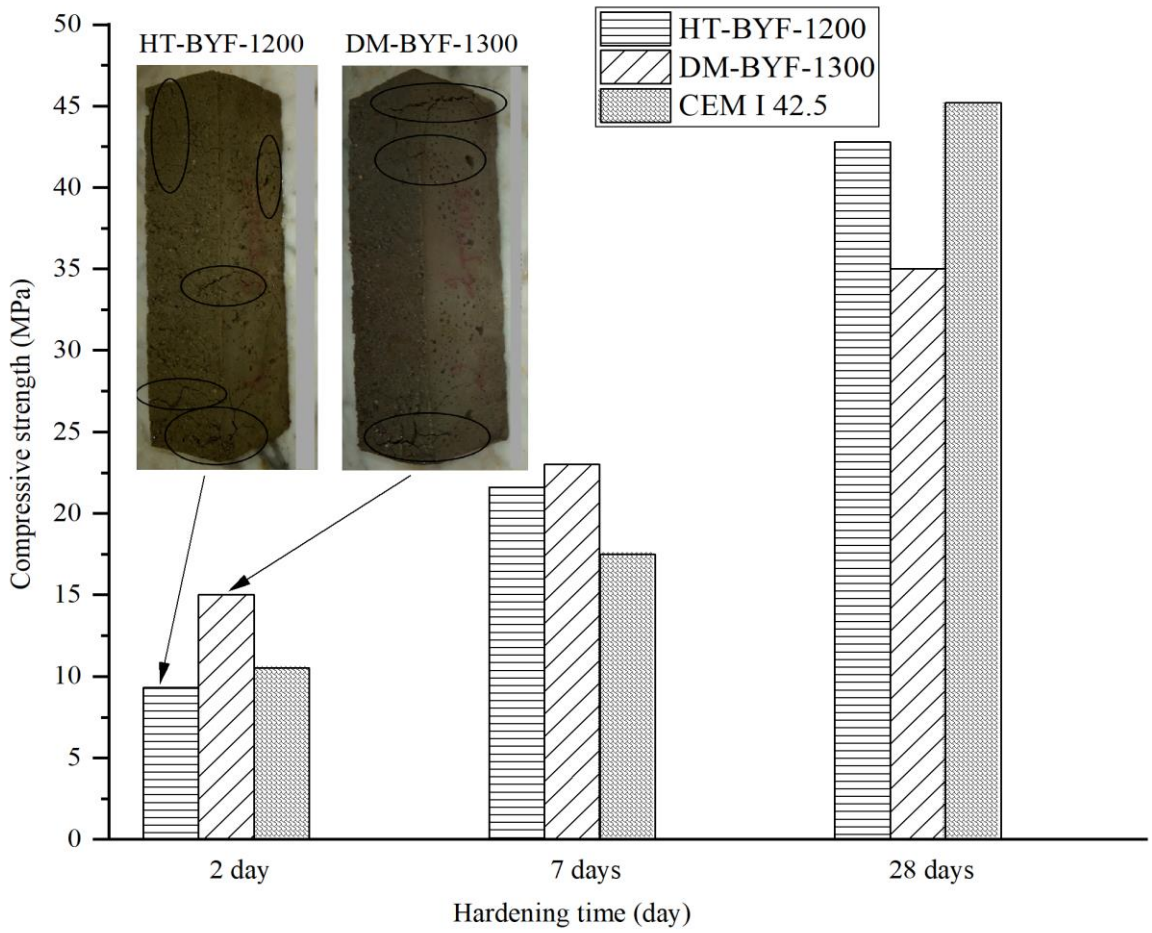

Figure 13. Compressive strength evolution with hardening time of HT-BYF-1200, DM-BYF-1300 and CEM I 42.5 mortars. Photographs showing cracks in mortars of HT-BYF-1200 and DM-BYF-1300 mortars after 2 days of hardening

Supplementary Tables

Click here to view linked References

Click here to access/download

Supplementary Interactive Plot Data (CSV)

Tables S.docx

Supplementary Figures

Click here to view linked References

Click here to access/download

Supplementary Interactive Plot Data (CSV)

Figures S.docx

Highlights

The Highlights of this work, showing its originality, are mainly:

1- The nature of the used raw materials, composed from mixtures of hazardous wastes, posing an ecological problem in Algeria, and natural materials presents in abundance in this country.

2- The valorization of theses wastes and natural materials by using them to manufacture very reactive sulfoaluminate belite cement (BYF) at low burning temperature of important mechanical properties. The mixtures of wastes and natural materials in Algeria, containing the oxide sources of BYF cement, have never been used by other researchers.

3- The use of the hydrothermal method to manufacture very reactive BYF cement.

4- The careful characterizations, particularly with X-ray fluorescence (XRF), X-ray diffraction (XRD), coupled with Rietveld calculation method, thermal analysis (TGA-DSC), scanning electron microscopy (SEM) and isothermal calorimetry, which have been able to highlight all the minerals and their structures and textures despite the mineralogical complexity of the used raw materials. This allowed for rich scientific and rational interpretations that explained the mechanical performance.

5- The control of the hydrothermal treatment effect of mixture and the burning temperature of precursor on the clinkering process and the cement paste properties.

6- The obtaining of this eco-cement at low burning temperature (1200°C) with high mechanical strength (42 MPa after 28 days). This will allow this material to replace the conventional cement in the field of construction.